Proceedings of ASME Turbo Expo 2011
GT2011
June 6-10, 2011, Vancouver, British Columbia, Canada

GT2011-45014

Numerical Analysis of Effects of Centrifugal Compressor Impeller Design on Overall- and Flow Field Performance

A. Hildebrandt *, H. Franz [+], C. Jakiel *

* MAN Diesel & Turbo SE, Steinbrinkstraße 1, 46145 Oberhausen, Germany
[+]Institute of Jet Propulsion and Turbomachinery IST, RWTH Aachen, Germany

ABSTRACT

The present paper deals with two different subjects in the field of centrifugal compressors, namely impeller design and its aerodynamic analysis. The paper provides results of aerodynamic design of low specific speed centrifugal compressor impellers. The design objective is the improvement of the efficiency of a 2D-impeller by means of a 3D-impeller design. The design volume flow and isentropic pressure coefficient of the 3D-impeller should be similar to the one of the 2D-impeller. The numerical CFD (Computational Fluid Dynamics) analysis comprises non-dimensional results of overall impeller and stage performance as well as flow details (circumferentially averaged fluid properties in the impeller exit plane). Furthermore, the paper presents the analysis of secondary flow development of different impellers in comparison with a 2D-impeller of prismatic blade profile. The numerical analysis focuses on understanding of different development of the impeller secondary zone. Results show a direct correlation between the overall performance and secondary flow of the different impellers providing more insight into the aerodynamic philosophy of design of centrifugal compressor impellers.

NOMENCLATURE

A, A_s	Area, secondary flow area [m^2]
C_m, $\overline{C}_m$	Absolute (averaged) meridional velocity [m/s]
D_2, D_4, D_N	Impeller-, diffuser outlet, hub-diameter [m]
DR_p	Impeller diffusion rate [-]
k_s	Separation factor (Jet wake model) [-]
$\dot{m}$, $\dot{m}_s$, $\dot{m}_{des}$	Mass flow, Secondary flow, design mass flow [kg/s]
$W_{1,tip}$, W_{2p}	Impeller inlet and outlet relative velocity of primary flow [m/s]
n, b, z	Normal, binormal and axial intrinsic coordinate [-]
N, N_{des}	Rotational (design) speed [RPM]
R_n, R_b	Meridional curvature, Blade curvature [1/m]
SV	Secondary vorticity [1/s]
α_2, α_4	Abs. flow angle Impeller, diffuser exit [deg]
β_{2p}, $\beta_{2, Blade}$	Rel. Flow angle, impeller exit blade angle [deg]
η_{pol}, η_s	Polytropic and isentropic efficiency [-]
φ	Flow coefficient [-]
ψ_s	Isentropic pressure coefficient (psi_s) [-]
$\psi_i = \eta_s \psi_s$	Inner pressure coefficient (psi_i) [-]
ω	Total pressure loss coefficient [-]
Ω_s	Secondary vorticity [1/s]
Ω	Angular (shaft) speed [1/s]
ρ_{2p}	Fluid density primary flow [kg/m^3]
Θ, Theta	Circumferential (wrap) angle [deg]
$\chi = \frac{\dot{m}_s}{\dot{m}}$	Secondary mass flux ratio [-]
$\varepsilon = \frac{A_s}{A}$	Secondary flow area ratio [-]

INTRODUCTION

Low specific speed stages with medium flow coefficient being used in application of process and oil and gas industry, are specified to ensure aerodynamic requirements such as high peak efficiency and large operational range at certain predefined hub-to tip ratio. The centrifugal impeller is the key component of such compression stage, see **Figure 1** for a meridional and 3D view of an impeller example.

Impeller optimisation is considered as base of stage optimisation. In general, impeller optimisation may follow classical design rules based on 1D, 2D and 3D calculation methodology as can be found in the literature [1],[2],[[3],[4].

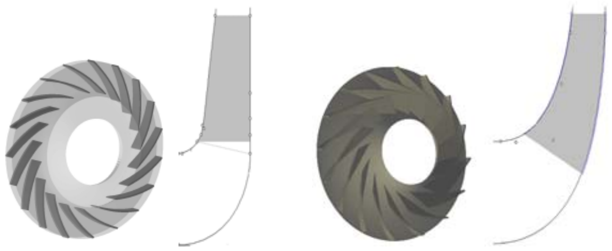

Figure 1 3D sketch and meridional sketch of the 2D impeller (left) and the RearLoad impeller (right) .

Despite modern impeller design methodology based on automatic multipoint, multi-objective aerodynamic (CFD) and mechanical (FEM) optimisation tools [5],[6],[7[,[8], classical impeller design is still applied in industry. Therefore, it may be recommended to keep analysis and understanding of centrifugal compressor impeller aerodynamics in focus [9]. In aerodynamic analysis, besides overall performance analysis, the evaluation of loss mechanism is of importance. Impeller losses can be divided into several groups: Recirculation work loss, disc friction, friction loss on wetted surface, incidence loss at impeller leading edge, diffusion loss and secondary loss (also called passage curvature loss) due to pressure gradients from hub to shroud arising from coriolis and centrifugal forces. Different loss mechanism may dominate, dependent on the impeller flow coefficient [4]. For medium flow coefficient impeller, however, passage curvature loss and friction loss may equal each other, which offers large freedom for blade loading of basic impeller design. Blade loading is considered as a key design parameter and is often defined in a range between rear and front loading. In general, effect of different loading type is well known, however seldom, profound detailed analysis is given to judge important issue such quantitative and qualitative secondary zone parameter. This paper aims at the evaluation of the secondary flux and the secondary vorticity for four different impellers. These four impellers have nearly the same overall design point pressure rise, design point flow coefficient, and nearly the same impeller outlet blade angle but comprise a different impeller loading. The first impeller features a front loading design (called FrontLoad- and FrontLoad_mod-impeller). The FrontLoad_mod-impeller comprises the same blade angle distribution and hub meridional contour line as the FrontLoad-impeller but features a constricted meridional shroud contour. The third impeller has a blade rear loading (called RearLoad-impeller). The last impeller features a prismatic 2D-blade design.

Table 1 gives an overview on the basic data such as blade number, and normalised outlet width and normalised outlet angle. While the 2D-impeller has 19 blades, the remaining impellers are designed with 16 blades. The secondary flow is effected by the type of blade loading and will be analysed in detail in this paper. Main focus is on analysis of flow field performance and secondary zone parameters.

Table 1 Normalised main data of the four different impellers.

	2D	RearLoad	Front-Load	Front-Load_mod
Blade number [-]	19	16	16	16
Outlet width norm. [-]	1	0.97 b_2(2D)	0.96 b_2(2D)	0.96 b_2(2D)
β_2 norm. [-]	1	1.033 β_2 (2D)	0.981 β_2 (2D)	0.981 β_2 (2D)

TWO DIMENSIONAL (2D)-NON-VISCOUS-BLADE CALCULATION

The geometry of the four different impellers are not allowed to be shown due to non-disclosure agreements. Instead of presenting the blade angle distribution and meridional contour lines, the results of non-viscid calculations are shown in **Figure 2** and Figure 3. These two figures give a good indirect estimate about the prinicpal differences in blade angle distriubution and the meridional contour lines. According to 2D (two-dimensional) non-viscous flow results in the blade to blade (S1) plane, the RearLoad impeller features a rear-blade loading with constant change of tangential velocity (*d(RCu)/dm* from 30% to 90% nondimensional meridional length, see **Figure 2**.

The tangential velocity gradient of the FrontLoad-impeller lays in between the one of the 2D- and the RearLoad-impellers. The tangential velocity gradient directly effects the static pressure rise as can be seen from **Figure 2**, where a steep pressure gradient across the meridional length is observed for both the 2D and FrontLoad-Impellers. The relative shroud Mach number in the first part of the non-dimensional meridional length of the RearLoad-impeller, in comparison to the 2D-impeller, is slightly reduced, see **Figure 3**. The shroud loading of the FrontLoad-Impeller is strongly reduced in the rear part of the meridional length on account of a fast diffusion in the first part of meridional flow path. At the hub, the loading is maximum at 20% to 60% meridional length.

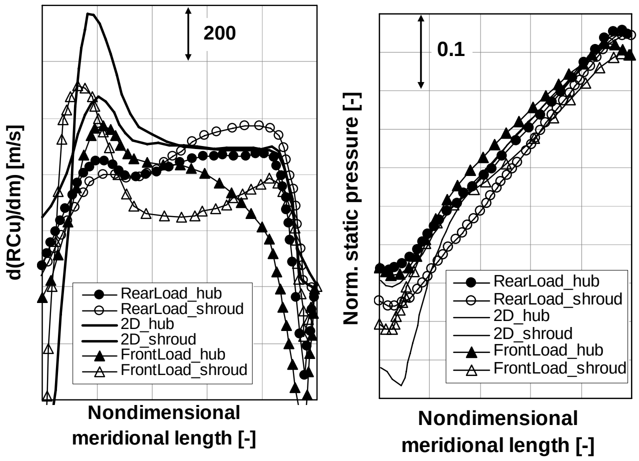

Figure 2 **2D-Non-viscous results: Pressure rise and blade loading of 2D-, RearLoad- and FrontLoad-impeller.**

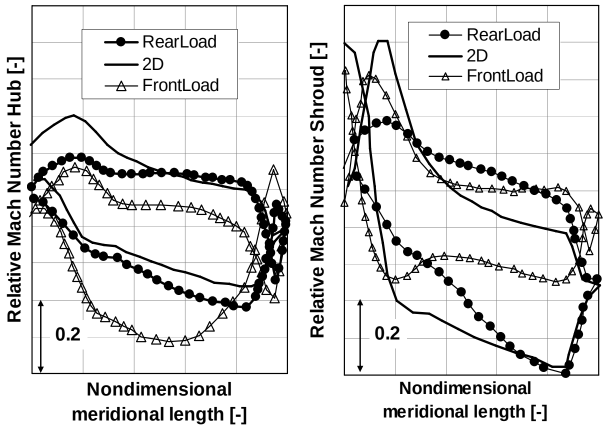

Figure 3 **2D-Non-viscous results: Relative Mach number of 2D-, RearLoad- and FrontLoad-impeller.**

The mean hub and shroud velocity is nearly the same for both the 2D and RearLoad-impellers but significantly reduced at hub for the FrontLoad-impeller while being increased at shroud. The reduced mean velocity (see **Figure 3**) and therefore reduced friction loss result in lower entropy production in operation towards the choke margin, whereas strong diffusion at both hub and shroud of the FrontLoad-impeller may give concern to strong risk of separation in operation near surge line.

THREE DIMENSIONAL (3D) VISCOUS CFD-IMPELLER-CALCULATION

Steady-State compressible turbulent Navier-Stokes calculations were performed with commercial Software NUMECA Fine Turbo. Details of the numerical methodology and grid quality are shown in **Table 2**. The grid generation comprised HOH-topology and orthogonality optimisation in order to maximise grid quality. Numerical boundary conditions at the inlet and outlet of the computational domain are total pressure, total temperature, flow angle and static pressure.

Table 2 Details of CFD numerical methodology and grid quality.

Turbulence model	Spalart-Allmaras/ kε Chien Low Re
Descretizsation	Central Difference Scheme
Total Residue [-]	Convergence Criteria: 10^{-3} to 10^{-4}
Grid Skewness [deg]	Min.19.4 deg, <36 deg: less 0.7%
Grid Aspect ratio [-]	>1000 for less 1.2% of total cells
Grid Max. Exp. ratio [-]	<3.5
Grid Cell number	Appr.665,000 points
Inlet	45 x 41 x 57 (pitch-,cord-, stream-wise)
Diffuser	85 x 41x 69 (pitch-,cord-, stream-wise)
Rotor	41 x 41 x 101 (main H-grid) 17 x 41x 177 (O- grid)

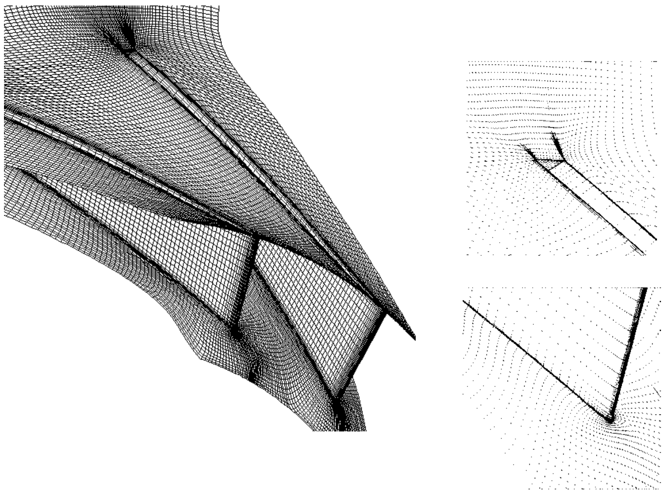

Figure 4 **NUMECA CFD-Grid Rotor-Leading edge and trailing edge details.**

A numerical study with three different grid densities (420,000, 665,000 and 1,050,000 grid points) has been performed with the RearLoad-impeller, see Figure 5, concluding that the model of medium grid density is sufficient to ensure grid independency. CFD Fine Turbo results predict a RearLoad-impeller total efficiency peak increase of approximately 1.5% in comparison with the 2D-impeller, see **Figure 6**. The choke margins of both the RearLoad- and Frontload-impeller are increased. The CFD predicted surge margin of the new impeller design does not satisfy the expectations, however according to previous experience with NUMECA software, the surge margin is underpredicted. In comparison with the RearLoad- and 2D-impeller, the CFD predicted surge margin of the original FrontLoad-impeller is smaller. The 1D-mass averaged flow angles α_2 and α_4 near numerically predicted surge (horizontal gradient of stage pressure coefficient), are shown in **Figure 7** in order to judge the risk of vaneless diffuser stall.

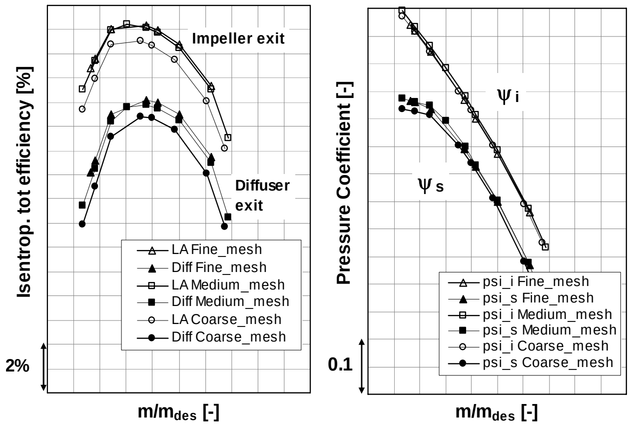

Figure 5 Results of grid independence study: Left: Total isentropic efficiency at impeller and diffuser exit, right: Work and isentropic pressure coefficient.

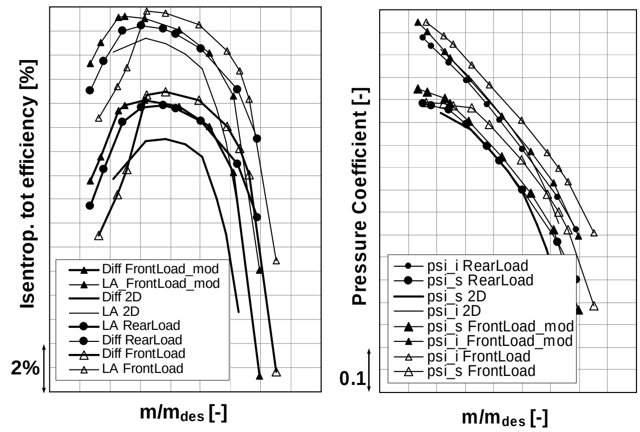

Figure 6 **CFD-calculations: Comparison between the 2D-, RearLoad, FrontLoad- and FrontLoad_mod-impeller. Left: isentropic tot efficiency at impeller outlet (LA) and diffuser outlet (Diff), right: Isentropic stage work coefficient and ideal stage work coefficient.**

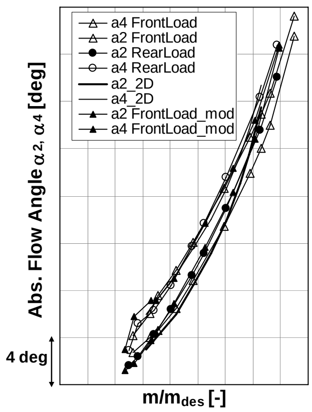

Figure 7 **CFD calculated absolute flow angle at impeller and vaneless diffuser exit: Comparison between the 2D, RearLoad, FrontLoad and FrontLoad_mod impellers. Terms a2 and a4 denote the flow angle at impeller exit and diffuser exit, respectively.**

The impeller exit flow angle does not reach a lower value than 15 degree being equal to the Kobayashi diffuser stall criteria [11]. Although the outlet metal angles of all impellers are rather close to each other (differences range from -1.9% to 3.3%, see **Table 2**), the pressure coefficient of the FrontLoad-impeller outperforms the RearLoad-impeller. The aerodynamic superior behaviour of the RearLoad-impeller over the 2D-impeller can be also identified by analysis of the flow details such as the relative Mach number at impeller inlet. Similar to the predicted 2D-non-viscous results, the relative inlet Mach number of the 2D-impeller at both hub and shroud is significantly higher than for the RearLoad-impeller, see **Figure 8**. Since the impeller exit relative Mach number is nearly the same for both impellers, diffusion ratio and therefore the risk of flow separation for the RearLoad-impeller is lower than for the 2D-impeller. The relatively strong diffusion of the 2D-impeller directly effects the static pressure rise, similar as predicted by 2D-non-viscous calculation. In contrast to the 2D-impeller results, CFD shows a smooth pressure rise for the RearLoad-impeller, see **Figure 2**.

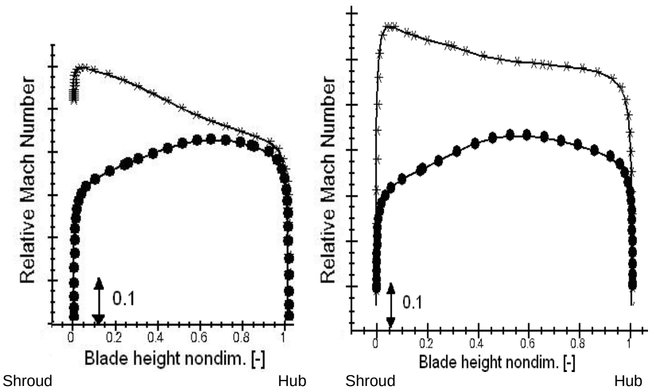

Figure 8 **CFD-predicted relative Mach number at impeller inlet and exit at design speed and in design point: Left: RearLoad-impeller, right: 2D-impeller, circle symbols: outlet, cross symbols: inlet. Same scale of ordinate-axis is used for both sub-figures.**

Impeller and Diffuser Plane Analysis

For detailed comparison of the different impellers, the analysis comprises circumferentially mass flow averaged flow properties such as entropy, Mach number and absolute flow angle. These fluid properties were investigated at three different operational points: the design point (**Figure 9**), one operational point near choke line (**Figure 10**) and one point near surge (**Figure 11**). For the flow field analysis at three different operational points, all four impellers have been analysed at similar mass flow, see **Table 3.** For the 2D-impeller, due to numerical instability, a CFD calculation at a nondimensional mass flow lower than 0.81 could not be performed. The following conclusions can be drawn for analysis at impeller exit in the design point (**Figure 9)**: The RearLoad- and FrontLoad-impeller feature absolute flow angle profiling being more dominant near hub while the 2D-impeller show a rather symmetric flow angle profile with maximum peak at 50% blade height where the minimum of Mach number can be found for all four impellers. Consequently, the 2D impeller shows a rather flat meridional flow velocity and therefore rather uniform mass flux distribution over blade height in contrary to the RearLoad- and FrontLoad-impellers.

Table 3 Base of comparison at different nondimensional operational mass flow.

	2D	RearLoad	Front-Load	Front-Load_mod
Surge	0.81	0.78	0.76	0.77
Design	0.98	0.98	0.98	0.98
Choke	1.22	1.23	1.22	1.21

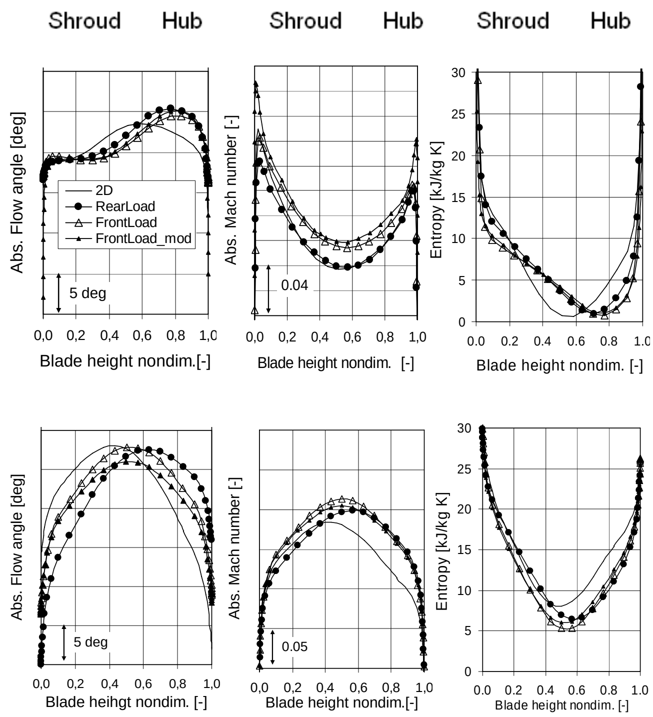

Figure 9 **Circumferentially mass averaged flow properties in design point. Top: evaluation plane impeller exit (D=1.05 D_2), bottom: evaluation plane vaneless diffuser exit (D=1.65 D_2).**

For the 2D- impeller, the non-weighted entropy distribution shows a significant minimum at 50% while for the other impellers, the minimum entropy is shifted towards the hub wall (**Figure 9).** Performing an area weighted averaging, would yield in the same efficiency for all four impellers, whereas mass flow averaging clearly brings forward the superiority of the 3D designed impeller in terms of entropy minimisation. At diffuser exit, the differences between the four impellers become stronger in terms of flow angle distribution but not in terms of maximum flow angle. For the 2D-impeller, the flow angle peak is located towards the shroud wall accompanied with a strong downfall towards the hub, whereas for the RearLoad-impeller, peak is located at 60% blade height with lowest values (Minimum=10°) towards the shroud wall The flow angle distribution of the FrontLoad-impeller is in between those of the RearLoad- and 2D-impeller being also more uniform. The Mach number distribution for the four impellers is rather similar with peak at 45-55% blade height. The 2D-impeller shows the lowest peak Mach number, however accompanied with strongly reduced values near hub wall.

For the impeller analysis near choke condition, the absolute flow angle, absolute Mach number and specific entropy are presented in **Figure 10**. Both the 2D and FrontLoad_mod-impeller indicate a rather high peak of absolute flow angle at

60% blade height, whereas for the RearLoad- and FrontLoad-impeller, the flow angle peak is reduced by 5-10 degree. The FrontLoad-impeller provides the most uniform flow angle distribution at both impeller and diffuser exit of all four impellers. The main reason for the low overall efficiency of the 2D-impeller is the relatively high entropy rate near shroud which comes along with a rather low flow angle near shroud. The RearLoad-impeller gives the lowest flow angles near shroud among the four impellers with relatively high circumferential velocity component. This is the reason for the relatively higher entropy rate from shroud wall up to 50% blade height. The diffuser outlet flow of the 2D-impeller features the strongest mixing process with strong redistribution of flow angle having a more uniform outlet flow angle at diffuser exit. For the RearLoad-impeller, there is further enhancement of the flow angle non-uniformity.

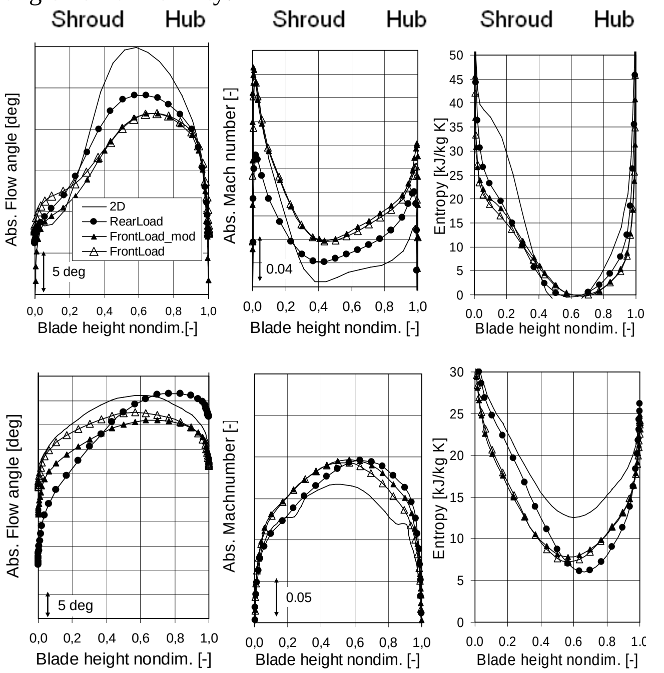

Figure 10 Circumferentially mass averaged flow properties near choke point. Top: evaluation plane impeller exit (D=1.05 D_2), bottom: evaluation plane vaneless diffuser exit (D=1.65 D_2).

Comparing the absolute flow angle of the RearLoad- and FrontLoad-impeller, the flow inlet conditions into the downstream return channel vane system seem superior for the FrontLoad-impeller. As expected from the low overall performance, the 2D-impeller shows high entropy rate over the entire blade height since already operating close to choke while for the 3D-impellers, this operational point is still away from choke flow.

All impellers feature the similar qualitative and quantitative impeller outlet flow angle near surge operation, see **Figure 11**. The 2D and RearLoad-impeller show slightly lower absolute values of Mach number distribution than both FrontLoad-impellers. The flow separation of the FrontLoad-impeller can only be recognised by the increased entropy values over the blade height but not by the Mach number distribution.

At the diffuser outlet, there is a significant difference between the FrontLoad-impeller and the remaining impellers: While the FrontLoad-impeller shows a very symmetric Mach number distribution, for all three other impellers, flow is almost detached towards the hub wall. There is no clear explanation for this asymmetric flow angle distribution except for the fact, that already at impeller exit, for the FrontLoad-impeller, Mach number distribution was most uniform.

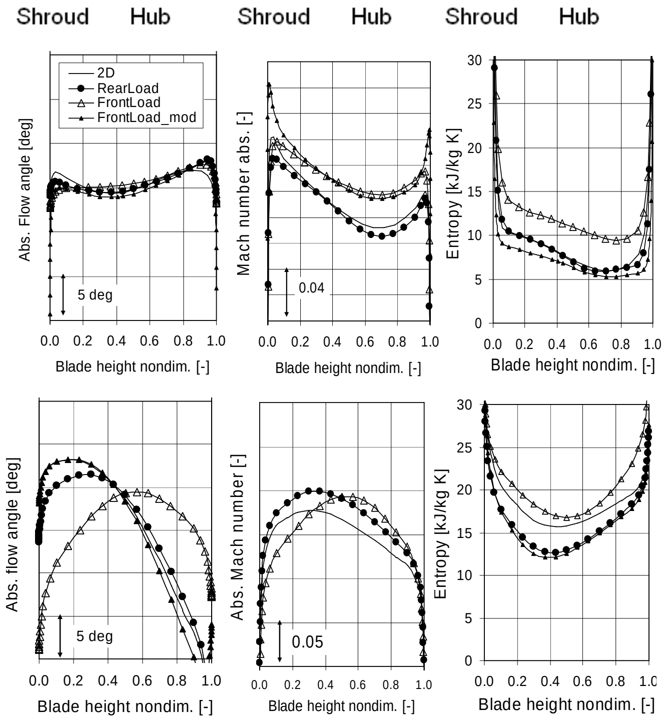

Figure 11 Circumferentially mass averaged flow properties near surge operation. Top: evaluation plane impeller exit (D=1.05 D_2), bottom: evaluation plane vaneless diffuser exit (D=1.65 D_2).

Consequences from the analysis of 1D averaged flow properties regarding the inlet flow into the return channel system: it seems, that despite the fact of low performance near surge point, the FrontLoad-impeller provides the most uniform diffuser outlet flow angle, followed by the FrontLoad_mod-impeller while the RearLoad-impeller shows the most non-uniform flow angle distribution, especially near choke flow condition. The more uniform flow angle distribution of the FrontLoad-impellers offers reduced total pressure loss within the downstream U-Turn, where due to potential flow field effect, the flow near the shroud casing wall is highly prone to separate.

Analysis of Flow Field Pattern

The flow field of a shrouded impeller slightly differs from the flow field of an open impeller such that interaction of tip clearance flow with the wake flow (imposed by Coriolis and Centrifugal forces) is missing. In Ziegler et al. [14],[15], L2F (Laser Two Focus) measurements in the impeller exit plane of a non-shrouded (open) impeller identified a velocity wake pattern (by means of meridional velocity and absolute flow angle) that spanned from suction side into the center of flow field being less concentrated towards the suction side corner than i.e. for the four shrouded impellers discussed here.

Comparing the tangential velocity distribution of all four impellers, similar flow patterns can be observed at design point, see **Figure 12**. In general, the local peak efficiency in impeller exit plane correlates with minimum tangential velocities. The regions of high tangential velocity suffer from high entropy or low efficiency, respectively. As common for centrifugal impellers, highly efficient flow exist in a region towards the pressure side.

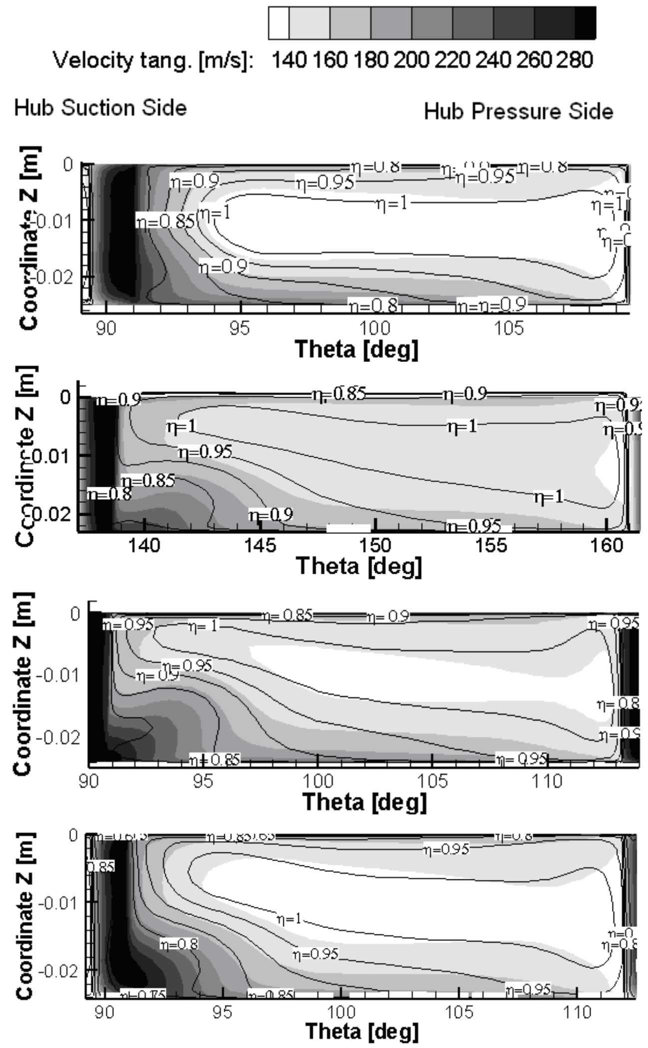

Figure 12 **CFD results: Tangential velocity and locally calculated efficiency in S3 plane at impeller exit (D=1.01 D_2) in design point. From top to bottom: 2D-, FrontLoad-, FrontLoad_mod and RearLoad-impeller at N/N_{des}=1.0 in design point.**

In case of a 2D-impeller, the flow pattern of tangential velocity and efficiency is rather symmetric. Here, the (efficiency) wake is present near the suction side over the whole blade height, whereas for the 3D impellers the wake is concentrated in the shroud suction corner. The FrontLoad-impeller shows a reduced region of high tangential velocity component compared to the RearLoad-impeller where the shroud suction side wake span from the corner to nearly 1/3 of the blade height, being more concentrated inside the corner. The superiority of the FrontLoad-impeller over the 2D and rear-load impeller is clearly identified, as shown by the isentropic lines η=0.9 and η=0.85 in **Figure 12.**

Analysing the meridional component and flow angle in the impeller exit plane (see **Figure 13**), further differences between the four different impellers are realised: The FrontLoad- and FrontLoad_mod-impeller feature the peak of highest absolute flow angle to be located closer to suction side and hub wall than the RearLoad- and 2D-impeller.

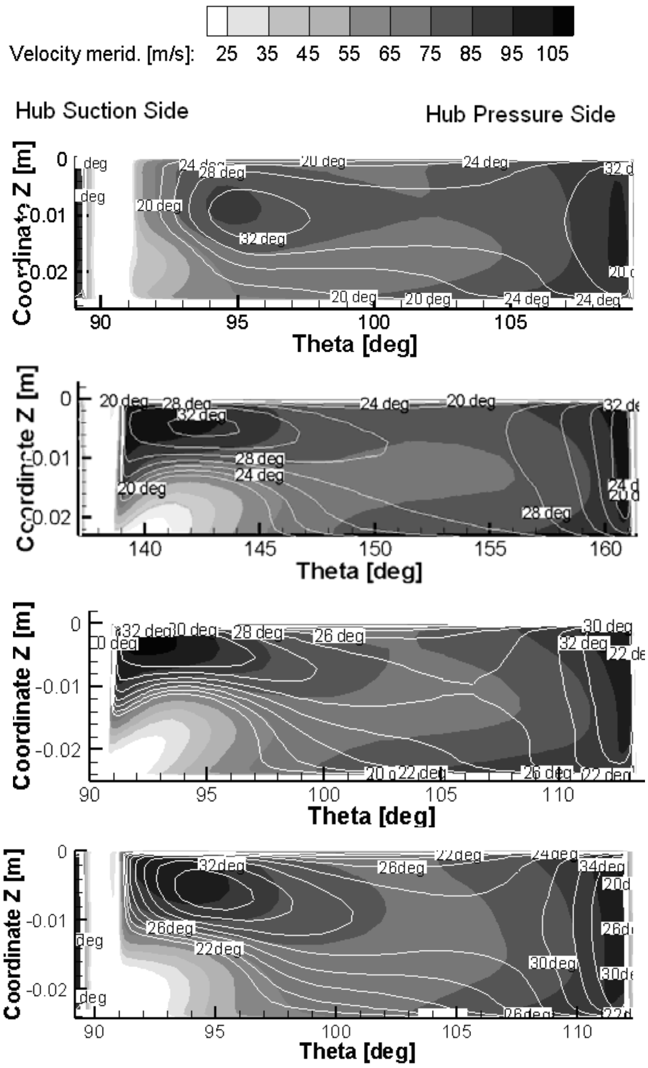

Figure 13 **CFD results: Meridional velocity and absolute flow angle (shown as white isolines) at impeller exit (D=1.01 D_2) From top to bottom: 2D-, FrontLoad-, FrontLoad_mod-, and RearLoad-impeller at N/N_{des}=1.0 in design point**

The meridional velocity wake and jet area close to the suction side is very pronounced for the 3D-impellers in contrary to the 2D-impeller, whose velocity peak is slightly moved towards the blade center. The meridional velocity wake of the FrontLoad- and FrontLoad_mod-impeller is somewhat tilted and does not span the entire corner as for the RearLoad-impeller.

Secondary Loss Analysis

For the analysis of flow losses in the S3 plane, the flow field is separated into a primary and a secondary zone. According to the definition by Japikse [3], the flow in the primary zone is nearly isentropic while the secondary zone comprises all fluid losses. Another definition of secondary zone can be found in Eckardt [13]: Here, the two zones are described as jet and wake. For quantitative calculation of the two zones, one flow property is chosen as zone separation criterion. Then, one isoline of this variable represents the border between the primary and secondary flow. Dependent on these two definitions there are two different separation variables in this paper: first the local isentropic efficiency (see **Eq. 2**) to account for secondary zone definition according to Japikse, as has already been applied in Hildebrandt and Genrup **[12]** and secondly the meridional velocity (see **Eq. 3**) according to the definition by Eckardt.

$$\dot{m}(1-\chi) = (1-\varepsilon)\rho_{2p} W_{2p} A \cos\beta_{2p} \qquad \text{Eq. 1}$$

$$if\ \left[\eta(\Theta, z) \le (1-k_s)\overline{\eta}\right] \quad then \quad \dot{m} = \dot{m}_s \qquad \text{Eq. 2}$$

$$if\ \left[C_m(\Theta, z) \le (1-k_s)\overline{C}_m\right] \quad then \quad \dot{m} = \dot{m}_s \qquad \text{Eq. 3}$$

For analysis described below, 98% of averaged efficiency and 90% of meridional velocity C_m is taken for border definition between the zones. Areas with a local value below the separation value are assigned as secondary zone. One dimensional parameters like secondary area ratio ε or secondary mass flow ratio χ are (see **Eq. 1**) calculated versus non operational mass flow.

Effects of Impeller Geometry In **Figure 13,** flow fields in the S3 planes of the different impellers are plotted. Obviously, there is for all impellers an area of very low meridional velocity on the suction side. This area represents the secondary zone, which is not similar for all impellers analysed. The development of low kinetic energy zones depends on the acting forces, which are influenced by the blade geometry. Development of secondary area ratio over a speed line (see **Figure 14**) is similar for all geometries. Thereby the separation criterion does not play a role for the basic form of the curve. Only the absolute value is influenced.

In general, secondary flow area fraction and secondary flux qualitatively follow the efficiency curves, having a minimum near the same flow coefficient as the peak efficiency. In comparison with the 3D-impellers, the 2D design has a reduced secondary area near design point operation m/m_{des}=1 (C_m-based according to **Eq. 3**), while with help of efficiency based criteria, secondary flow area is slightly above the one of the RearLoad-impeller. The relatively good performance of the 2D-impeller may surprise, however one has to consider, that the 2D-impeller blade loading is lower than for the 3D-impeller due to higher blade number. Towards choke, the superior characteristics of the RearLoad- and FrontLoad-impellers overweight the 2D-impeller secondary flow performance in both criteria of flow area fraction and flux fraction, see **Figure 14.**

Because of the horizontally positioned leading edge (see **Figure 1**), the 2D-impeller suffers higher incidence loss than the 3D-impellers. This higher incidence results in thicker boundary layers on the blade suction and pressure side which makes the secondary flow rise up. Associated to this effect, boundary layer thickness at blade leading edge is enlarged. From the onset of blading more low kinetic energy fluid is present and is pushed into the secondary zone. The wrapped blade leading edge of the 3D-impellers prevents large incidence angles and diminishes development of secondary zone. **Figure 14** verifies this assumption.

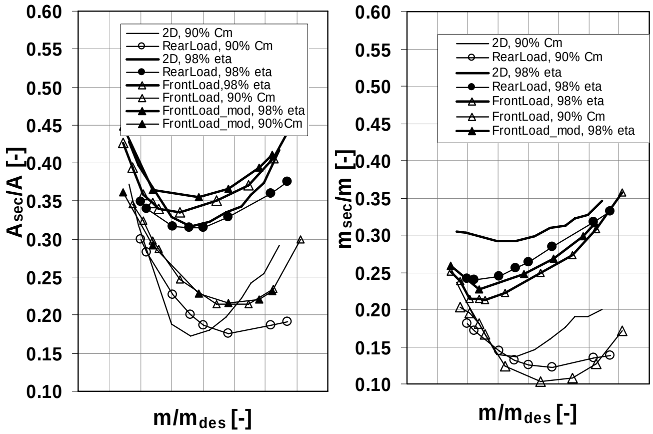

Figure 14 Secondary flux fraction and secondary flow area fraction of 2D, RearLoad, FrontLoad and FrontLoad_mod-impeller as function of operational mass flow at N=N_{des}.

As the secondary zone is the main source of flow losses, the mean efficiency in the impeller exit plane decreases with growing secondary mass flow ratio. Near design point operation primary zone, flow is mainly describing the flow characteristic. Therefore the parameter diffusion ratio and deviation angle are defined (**Eq. 4** and **Eq. 5**) as

$$DR_p = \frac{W_{1,tip}}{\overline{W}_{2,p}} \qquad \text{Eq. 4}$$

$$\delta_{2,p} = \beta_{2,Blade} - \overline{\beta}_{2,p} \qquad \text{Eq. 5}$$

The diffusion ratio represents the deceleration of the flow. The flow can only stand a certain deceleration before separation. According to **Figure 15**, the diffusion ratio of the 2D-impeller is increasing rapidly towards smaller flow rates. In comparison to the 3D-impeller the maximum diffusion ratio is reached at higher $m/m_{des,}$ thereby narrowing the operational range towards surge.

The behaviour of wake-tilt can be observed more clearly from the secondary vorticity pattern, see **Figure 16**. Here, the hub suction side corner is completely covered by a negative secondary vortex. Secondary vorticity SV is defined by **Eq. 6** being slightly different to other literature [19], where secondary vorticity is based on the dot product of mean velocity vector times rot C.

$$SV(\Theta, z) = \vec{C}(\Theta, z) \cdot rot\vec{C}(\Theta, z) \qquad \text{Eq. 6}$$

Analyzing the secondary vorticity of the four different geometries near impeller exit, one can observe only small differences between the RearLoad- and both FrontLoad-impellers, but a bigger deviation for the 2D-impeller, see **Figure 16**. In general, for all impellers, 3 different regions of main secondary vorticity are identified, whereas two of them are due to passage vorticity near hub and shroud wall.

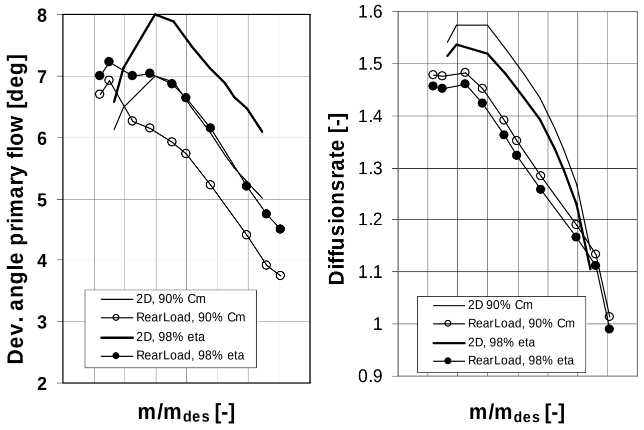

Figure 15 Deviation angle and diffusion rate of primary flow of the 2D and RearLoad-impeller as function of operational mass flow at N=N$_{des}$.

In **Figure 16,** positive secondary vorticity refers to rotation in clockwise direction and negative vorticity to counter-clockwise direction. One small negative vortex is located in the shroud suction corner, which in case for the 3D-impellers is oriented towards the center of channel. According to **Eq. 7** streamwise vorticity (dot product of vorticity and intrinsic streamwise coordinate s, see Lakschminarayana and Horlock [16], Brun and Kurz [17]) is dependent on the geometry (normal curvature R_N, binormal curvature R_B) and velocity gradients. In case of 2D-impeller, due to infinitely low meridional curvature R_N, the first term on right side of **Eq. 7** vanishes which is one reason for relatively low secondary vorticity and therefore rather small secondary flow fraction.

$$\frac{\partial}{\partial}\left[\frac{\Omega_S}{W}\right] = \frac{2}{W}\left[\frac{1}{R_N}\frac{\partial W}{\partial b} + \frac{1}{R_B}\frac{\partial W}{\partial n} + \frac{2\Omega}{W}\frac{\partial W}{\partial z}\right] \qquad \text{Eq. 7}$$

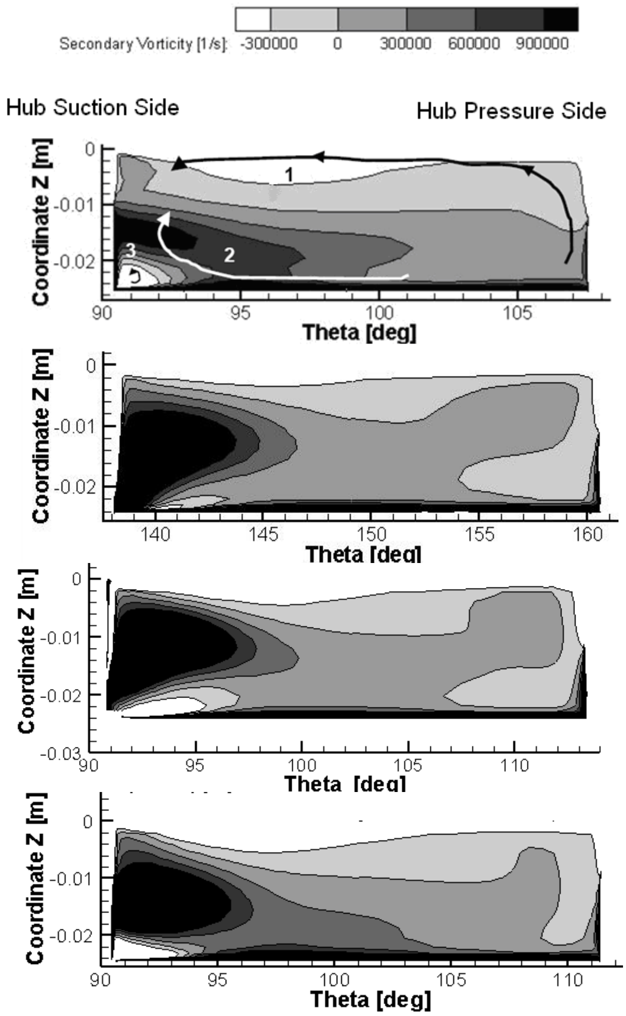

Figure 16 CFD results: Secondary Vorticity at impeller exit :From top to bottom: 2D-impeller, FrontLoad-, FrontLoad_mod- and RearLoad-impeller at N/N$_{des}$=1.0 in design point.

Effects of Shroud Leakage Modelling All numerical results presented so far have been achieved by CFD calculations without modelling of the shroud leakage flow. In case that an absolute flow pattern downstream the impeller is aimed for (i.e. for a vaned diffuser design) the question arises if the effects of more detailed CFD modelling on the outlet flow are similar to those effects due to different geometry as discussed before in the present paper. For that reason the RearLoad-impeller has been additionally modelled with the shroud leakage flow. The modelling topology of shroud leakage comprises of a series of H-type meshes, see **Figure 17**. Although there is efficiency decrease also by the rear hub plate, this effect is not considered here, since this leakage flow will not effect the impeller flow field. The effect of shroud leakage flow on flow field is as follows: The boundary layer flow inside the impeller is increased and shifted towards the hub wall. The mixing of leakage flow and core flow is dependent on the type of flow orientation between leakage and core-flow, see Mischo et al. [18], who investigated the effect of leakage re-entry on shroud separation.

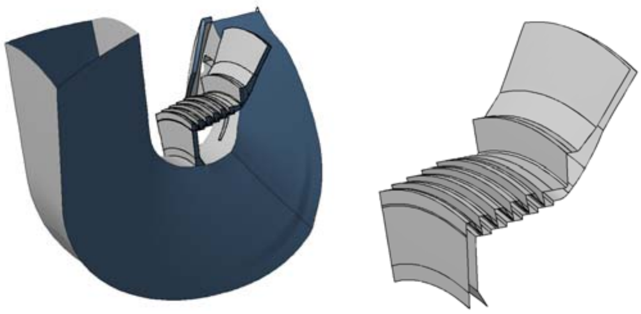

Figure 17 **CFD modelling of shroud leakage geometry.**

Analysis of the CFD results only show a minor effect of shroud leakage modelling on secondary zone flux fraction and secondary flow area fraction, see **Figure 18.** While differences in the secondary mass flux are almost negligible, discrepancy of the secondary mass flow area is in range of 0.02 to 0.05 being slightly higher in case evaluated on efficiency.

Figure 19 and **Figure 20** show the differences in meridional-, tangential flow field, efficiency and absolute flow angle, based on shroud leakage and non-leakage modelling methodology. The modelled shroud leakage generates a lower efficient area near shroud wall and turns the center of high efficiency isolines towards the hub wall. Furthermore, the low efficiency in the shroud suction side corner is significantly more dominant in the calculations with modelled shroud leakage. While in the shroud suction side corner of non-leakage modelled geometry, absolute flow angle is reduced, in the remaining absolute flow is marginally steepened due to elevated meridional velocity component.

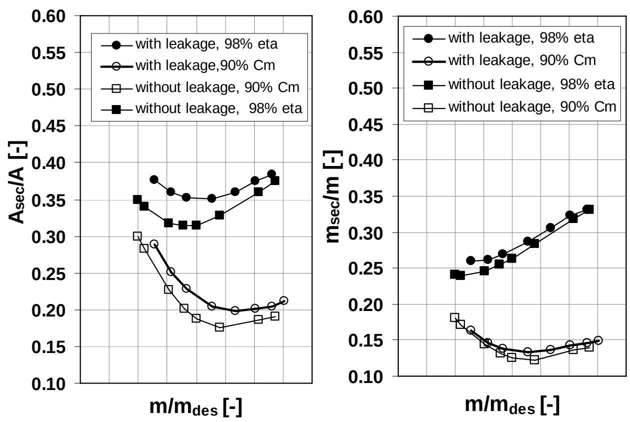

Figure 18 **Effect of shroud leakage modelling on secondary flux and secondary flow area and deviation angle, RearLoad-impeller at N/N_{des}=1.0.**

Since the wake zone is raised in case of shroud modelled geometry, the turbulence viscosity level is increased in the shroud suction side corner in the place of maximum shear due to secondary vorticity, see **Figure 21**. Interestingly, in case of non-modelled leakage, the maximum turbulent viscosity is located near the hub pressure side corner, while being reduced towards the velocity wake zone. The effect of shroud modelling on the secondary flux performance is independent on the impeller blade geometry.

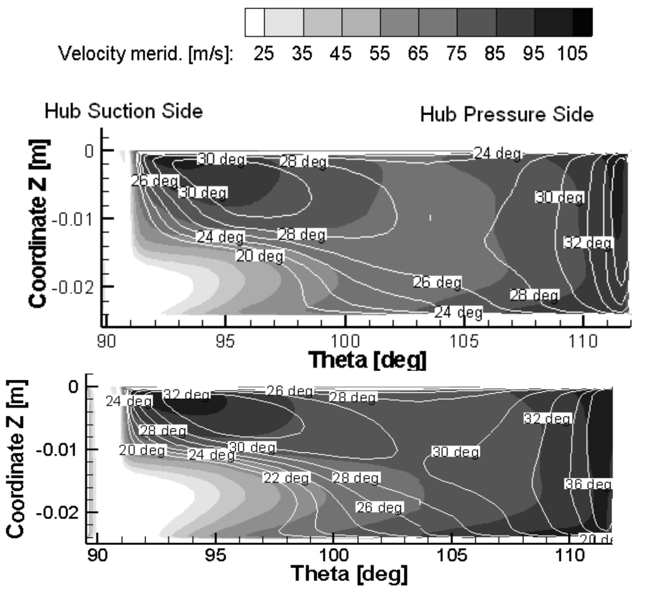

Figure 19 **Absolute flow angle and meridional velocity in impeller exit plane of RearLoad-impeller near design point, top: without shroud leakage modelling, bottom: with shroud leakage modelling.**

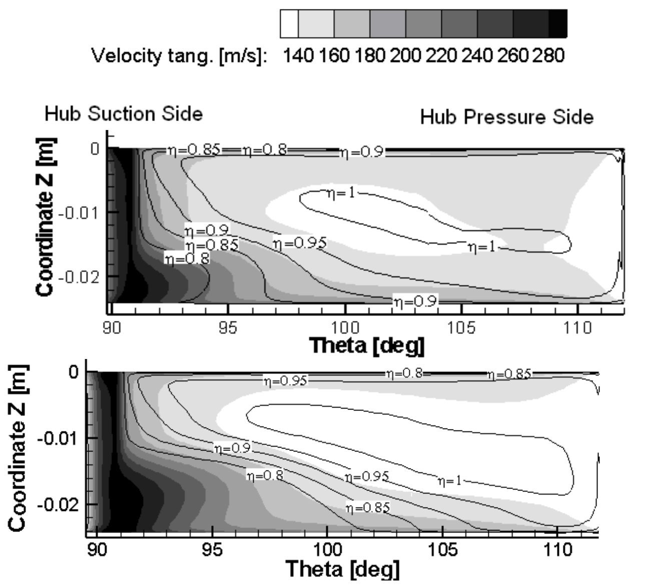

Figure 20 **Isentropic efficiency and tangential velocity in impeller exit plane of RearLoad-impeller near design point, top: without shroud leakage modelling, bottom: with shroud leakage modelling.**

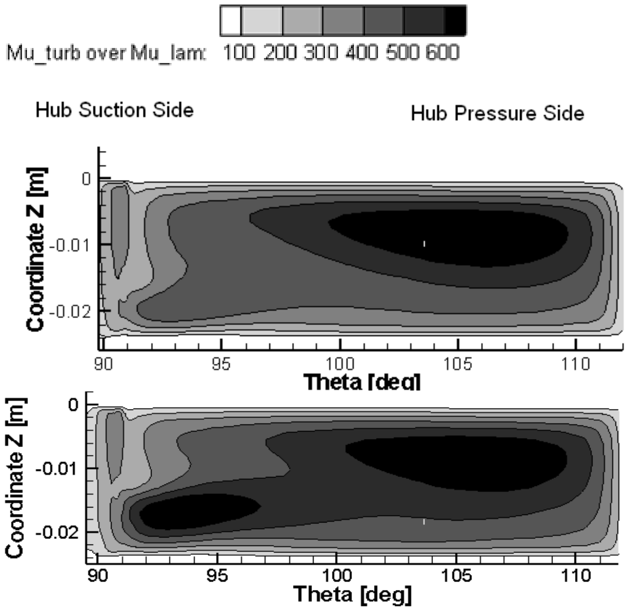

Figure 21 **Ratio of turbulent to laminar viscosity in impeller exit plane of RearLoad-impeller near design point, top: without shroud leakage modelling, bottom: with shroud leakage modelling.**

CONCLUSION

A comparison of centrifugal compressor design has been performed based on numerical calculations. Calculation results have shown the effect of different meridional curvature, 3D geometry effect on overall aerodynamic and flow field performance. For medium flow coefficient impellers with specification as relevant for impellers presented here, the secondary flow development is qualitative similar. In design point, the FrontLoad-impeller provides higher secondary flow area but lower secondary flux than the RearLoad- and 2D-impeller. Since for medium flow coefficient impellers, the different loss mechanisms such as secondary flow loss, diffusion loss and friction loss balance each other, there is no clear superiority of one blade loading type on the other, as could be presented here. For higher or lower flow coefficient either diffusion or friction loss may dominate such that one specific blade loading type may be preferred. Different development of secondary zone is explained by different meridional and blade curvature that effect the secondary vorticity and secondary zone parameter as numerically verified. The results of secondary zone quantification depend on level of geometry modelling (i.e. including or excluding shroud leakage modelling), the geometry of impellers but also the definition of secondary zone parameter, being either based on evaluation of local efficiency or meridional velocity. For verification of numerical results of the overall performance, the FrontLoad_mod-impeller and the RearLoad-impeller are going to be experimentally tested in future.

ACKNOWLEDGEMENTS

The investigations were conducted as part of a research program in the frame of AG Turbo. The work was supported by the Bundesministerium für Wirtschaft und Technologie (BMWi) as per resolution of the German Federal Parliament. The responsibility for the content lies solely with its authors. The authors would like to thank MAN Diesel & Turbo SE for their support and also for granting permission to publish results. Professor Van den Braembussche and Mr Prinsier from the Von Karman Institute For Fluid Dynamics VKI, Belgium, are gratefully acknowledged for contribution of the Front-Load-impeller design and discussion and general discussion.

REFERENCES

[1] Eckert, B., „*Axialkompressoren und Radialkompressoren*", Springer Verlag Berlin/ Göttingen/ Heidelberg 1953.

[2] Lüdtke, K.H., „*Process Centrifugal Compressors", Basics, Function, Operation, Design, Application*", Springer Verlag Berlin Heidelberg New York 2004.

[3] Japikse, D., "*Centrifugal Compressor Design and Performance"*, Concepts Eti, Inc. 1996.

[4] Aungier, R.H., "*Centrifugal Compressors, A Strategy for Aerodynamic Design and Analysis*", ASME Press, New York, 2000.

[5] Kim, J.-GH, Choi, J.H., Kim, K.Y., "*Design Optimization of a Centrifugal Compressor Impeller using Radial Basis Neural Network Method*", Proceedings of ASME Turbo Expo 2009, Orlando, GT-2009-59666.

[6] Bonaiuti, D., Arnone, A., Ermini, M., Baldassarre, L., "*Analysis and Optimization of Transonic Centrifugal Compressor Impellers Using the Design of Experiments Technique*", Proceedings of ASME TURBO EXPO 2002, Amsterdam, GT-2002-30619.

[7] Verstraete, T., Alsalihi, Z., Van den Braembussche, R.A. „*Multidisciplinary optimisation of a radial compressor for micro gas turbine applications"*, GT2007,- 27484, Proceedings of GT2007, ASME Turbo Expo 2007, Montreal, Canada 2007.

[8] Van den Braembussche, R.A., *Optimisation of Radial Impeller Geometry*", In Design and Analysis of High Speed Pumps (pp.13-1-13-28) Educational Notes RTO-EN-AVT-143, Paper 13. Neuilly-sur-Seine, France: RTO.

[9] Ibaraki, S., Matsuo, T., Kuma H., Sumida, K., Suita, T., „*Aerodynamics of a Transonic Centrifugal Compressor Impeller"*, Proceedings of ASME Turbo Expo 2002, Amsterdam, GT-2002-30374.

[10] Van den Braembussche, R.A. , Prinsier, J. ,Alsalihi, Z., Verstraete, T., *"Optimization of a Low Volume Flow Radial Compressor Impeller"*, MAN Turbo AG Contract Report 2008-26 July 2008.

[11]Nishida, H., Kobayashi, H., Takagi, T. and Fukushima, Y., *"A Study on the Rotating Stall of Centrifugal Compressors (2nd Report, Effect of Vaneless Diffuser Inlet Shape on Rotating Stall)"*, Transactions Japan Society of Mechanical Engineers (B Edition), 54, (449), pp.589-594.

[12] Hildebrandt, A., Genrup, M., "*Numerical Investigation of the Effect of Different Back Sweep Angle and Exducer Width on the Impeller Outlet Flow Pattern of a Centrifugal Compressor With Vaneless Diffuser"*, ASME Journal of Turbomachinery 129, 421 (2007).

[13] Eckardt, D., 1975,*"Instantaneous Measurements in the Jet-Wake Discharge Flow of a Centrifugal compressor Im-*

peller", ASME .J. Eng. Gas Turbines power, 97, pp.337-345.

[14] Ziegler, K.U., Gallus, H.E., and Niehuis, R., *"A Study on Impeller-Diffuser Interaction—Part I: Influence on the Performance"*, ASME Journal of Turbomachinery 125, (2003), pp. 173-183.

[15] Ziegler, K.U., Gallus, H.E., and Niehuis, R., *"A Study on Impeller-Diffuser Interaction—Part II: Detailed Flow Analysis"*, ASME Journal of Turbomachinery 125, (2003), pp. 183-193.

[16] Lakschminarayana, B., Horlock, J.H., *"Generalized Expressions for Secondary Vorticity Using Intrinsic Co-Ordinates"*, J. Fluid Mech. (1973), vol. 59, pp. 97-115.

[17] Brun, K., Kurz, R., "*Analysis of Secondary Flows in Centrifugal Impellers*", International Journal of Rotating Machinery 2005:1, 45-52.

[18] Mischo, B., C. Seebass-Linggi, Ribi, B., Mauri, S., "*Influence of Labyrinth Seal Leakage on centrifugal compressor performance*", GT2009-59524, Proceedings of ASME Turbo Expo 2009, USA, June 2009.

[19] Weiß, C., Grates, D.R., Thermann, H., Niehuis, R., *„Numerical Investigation of the Influence of the Tip Clearance on Wake Formation Inside a Radial Impeller"*, GT2003-8279, Proceedings of ASME Turbo Expo 2003m USA, Atlanta, June 2003.